Nucleus-nucleus cross sections and the validity of the factorization hypothesis at intermediate and high energies*

Saul Barshay†
State University of New York at Stony Brook, Stony Brook, New York 11790

C. B. Dover and J. P. Vary
Brookhaven National Laboratory, Upton, New York 11973

(Received 18 April 1974; revised manuscript received 10 June 1974)

We use an impact parameter representation of the scattering amplitude to predict nucleus-nucleus and nucleon-nucleus total, reaction, and elastic cross sections at intermediate and high energies. We investigate the question of factorization for these quantities and find that factorization holds to 20% if the radii of the projectile and target nuclei do not differ by more than 50%. This fact and the gross violation of factorization when the nuclei are very different in size are interpreted in the context of a simple geometric model. The dependence of composite particle cross sections and factorization ratios on the size of the elementary nucleon-nucleon cross section σ_{NN}^T is investigated. It is shown that strict functional factorization for total and reaction cross sections in the impact parameter scheme only applies in the limit of a "weak" σ_{NN}^T, for which a single scattering approximation is valid. This situation is not realized in practice, and nucleus-nucleus cross sections are instead found to be close to a geometric limit for all but the lightest nuclei. The energy dependence of nucleus-nucleus cross sections is found to be negligible above 100 MeV/particle.

I. INTRODUCTION

There has recently been considerable interest in the study of high energy nucleus-nucleus collisions.[1,2] It has been suggested[2] that such composite particle interactions might shed some light on fundamental questions of particle physics, in addition to extending our knowledge of nuclear physics. If such a viewpoint is to be taken, it is important to first understand in some detail just what features of nucleus-nucleus cross sections are predicted by the conventional methods of nuclear theory. It is the goal of this paper to provide such a backdrop of theoretical results based on the familiar models of nuclear physics, without recourse to the more elaborate concepts of particle physics such as Regge poles and cuts and, in particular, the Pomeron. In this approach, nuclei are described as spatially extended spherical distributions of hadronic matter, with a radius and surface thickness obtained from electron scattering experiments. We thus assume that a *geometrical* description of nuclei is valid, even at high energies. The other ingredient in this approach is the elementary nucleon-nucleon cross section, which is also taken from experiment. Once these input quantities are specified, the nucleus-nucleus cross sections are calculated by using an impact parameter representation of the scattering amplitude. This part of the calculation follows well-established methods for obtaining composite particle cross sections.[3,4] The virtue of such an approach, if it is correct, is to permit a simple and intuitively appealing discussion of nucleus-nucleus cross sections in terms of two simple geometrical parameters, namely

$$x = \min(R_A/R_B,\ R_B/R_A)\,, \qquad y = AB\sigma_{NN}^T/\sigma_{AB}^G\,, \tag{1.1}$$

where A and B are the atomic numbers of projectile and target, R_A and R_B are rms nuclear radii, σ_{NN}^T is the elementary nucleon-nucleon cross section, and σ_{AB}^G is a geometric limit of the total cross section.

The factorization ratios defined by

$$r_{AB} = (\sigma_{AB})^2/\sigma_{AA}\sigma_{BB}\,, \tag{1.2}$$

where σ_{AB} refers to the elastic, reaction, or total cross section for the $A+B$ reaction, are also of interest.[5-7] We have numerically evaluated such ratios for a wide variety of nucleus-nucleus reactions, in order to see under what conditions the factorization hypothesis $r \approx 1$ is numerically valid. Order of magnitude deviations from $r \approx 1$ are observed in some cases, but are understandable in terms of a simple geometric limit

$$r^G = \frac{(1+x)^4}{16x^2}\,. \tag{1.3}$$

Note that $r^G \gg 1$ for $x \ll 1$, i.e., when the target and projectile vary greatly in size. The fact that $r \approx 1$ to within 20% for many reactions does not necessarily imply that high energy concepts such as the Pomeron are required for the description of such reactions. If $x \approx 1$, values $r \approx 1$ are also produced by the simple geometrical model of Eq. (1.3). In order to substantiate a given high energy model, it seems likely that unless the total cross sections and factorization ratios deviate significantly from the dictates of geometry, one must look at more detailed properties of the nucleus-nucleus interaction. In all likelihood, these gross features will be explainable within the framework of conventional nuclear physics, at least in the domain of energy presently accessible. A short report of the work described here is given in Ref. 8.

II. NUCLEUS-NUCLEUS SCATTERING AMPLITUDE

Since we are primarily interested in high energy nucleus-nucleus collisions, we work in the impact parameter representation, in which the elastic scattering amplitude $F_{AB}(q)$ for nucleus A incident on nucleus B assumes the form

$$F_{AB}(q) = -ik_{AB}\int_0^\infty J_0(qb)(e^{2i\chi_{AB}(b)} - 1)b\,db\,. \quad (2.1)$$

The amplitude F_{AB} of Eq. (2.1) can also be viewed as the optical limit of the Glauber theory.[3,9-11] In Eq. (2.1), $q^2 = 2k_{AB}{}^2(1-\cos\theta)$ is the four-momentum transfer squared, k_{AB} is the nucleus-nucleus relative wave number, and χ_{AB} is the nuclear phase shift function given by

$$\chi_{AB}(b) = \sigma_{NN}^T(E)(i+\beta)T(b)/4\,, \quad (2.2)$$

where

$$\beta \equiv \mathrm{Re}f_{NN}(E)/\mathrm{Im}f_{NN}(E)$$

and

$$T(b) = \int_{-\infty}^{\infty} dz \int d\vec{r}\,'\rho_A(\vec{r}-\vec{r}\,')\rho_B(\vec{r}\,')\,. \quad (2.3)$$

$\sigma_{NN}^T(E)$ is the nucleon-nucleon total cross section and ρ_A and ρ_B are the projectile and target densities normalized to A and B, respectively, and $f_{NN}(E)$ is a spin and isospin averaged nucleon-nucleon forward scattering amplitude taken at the energy per particle E of the projectile in the lab system. We have[12]

$$f_{NN}(E) = \lambda f_{np} + (1-\lambda)f_{pp}\,,$$
$$\lambda = (Z_A N_B + Z_B N_A)/AB\,, \quad (2.4)$$

where Z and N are proton and neutron numbers and f_{np} and f_{pp} are the neutron-proton and proton-proton forward scattering amplitudes, respectively. We assume that $f_{nn} = f_{pp}$. In writing Eq. (2.2), we make the zero range approximation for the nucleon-nucleon interaction. This seems justified in the present case, since the range of the nucleon-nucleon force (<1.4 fm) is small compared to the radii of most of the nuclei we consider. The error we introduce is partially cancelled by using densities obtained from electron scattering experiments without correcting for the finite size of the proton. In this approximation, the phase shift $\chi_{AB}(b)$ is thus a separable product of an energy dependent factor $\sigma_{NN}^T(E)$ and a thickness function $T(b)$ which contains all the information on the geometrical properties of the colliding nuclei.

The total, reaction, and elastic cross sections are given, respectively, by

$$\sigma_{AB}^T = 4\pi\int_0^\infty \{1 - e^{-2\,\mathrm{Im}\chi_{AB}(b)}\cos[2\,\mathrm{Re}\chi_{AB}(b)]\}b\,db\,,$$
$$\sigma_{AB}^R = 2\pi\int_0^\infty (1 - e^{-4\,\mathrm{Im}\chi_{AB}(b)})b\,db\,, \quad (2.5)$$
$$\sigma_{AB}^E = \sigma_{AB}^T - \sigma_{AB}^R\,.$$

Another quantity of interest is the slope b_{AB} of the elastic diffraction peak. This we obtain from the elastic scattering differential cross section $d\sigma/dt$ for small $t = -q^2$ via the equation

$$\frac{(d\sigma_{AB}^E/dt)}{(d\sigma_{AB}^E/dt)_{t=0}} = \left|\frac{F_{AB}(t)}{F_{AB}(0)}\right|^2 \overset{t\to 0}{\approx} e^{b_{AB}t}\,. \quad (2.6)$$

By making a Taylor expansion of $F_{AB}(t)$ about $t=0$, we obtain

$$b_{AB} = -\frac{k_{AB}}{2\,|F_{AB}(0)|^2} \times [\mathrm{Im}F_{AB}(0)\,\mathrm{Re}G_{AB} - \mathrm{Re}F_{AB}(0)\,\mathrm{Im}G_{AB}]\,,$$
$$G_{AB} = \int_0^\infty (e^{2i\chi_{AB}(b)} - 1)b^3 db\,. \quad (2.7)$$

The b^3 weighting in G_{AB} enhances the contribution of large impact parameters and thus b_{AB} is sensi-

TABLE I. Nucleon-nucleon cross sections and β values as a function of energy.

Lab kinetic energy (GeV)	σ_{np} (mb)	σ_{pp} (mb)	β_{pp}
0.10	68.0	32.0	1.87
0.52	35.22	34.03	0.550
0.65	38.45	42.90	0.443
0.80	39.61	46.76	0.144
0.90	39.61	47.34	0.0017
1.05	40.39	47.50	−0.073
2.1	43.14	44.45	−0.292
4.2	42.06	41.17	−0.330
7.0	41.3	40.0	−0.320
25.0	38.9	38.90	−0.154

TABLE II. Nuclear density parameters.

Nucleus	α	R (fm)
p	0	0.8
^{3}He	0	1.77
^{6}Li	0.33	2.41
^{9}Be	0.67	2.42
^{12}C	1.33	2.47
^{14}N	1.67	2.48
^{16}O	1.60	2.75
^{18}O	2.00	2.77

Nucleus	w	a (fm)	R_0 (fm)	R (fm)
^{4}He	0.445	0.327	1.01	1.71
^{24}Mg	−0.188	0.587	3.13	3.03
^{28}Si	−0.122	0.57	3.21	3.13
^{32}S	0	0.59	3.20	3.12
^{40}Ar	0	0.61	3.39	3.47
^{48}Ti	−0.02	0.56	3.82	3.60
^{58}Ni	−0.185	0.499	4.35	3.73
^{68}Zn	0	0.625	4.35	4.08
^{90}Zr	−0.086	0.57	4.86	4.26
^{120}Sn	0	0.575	5.32	4.64
^{140}Ce	0	0.51	5.82	4.86
^{197}Au	0	0.53	6.38	5.32
^{208}Pb	0.32	0.54	6.40	5.49

tive to the behavior of ρ_A and ρ_B in the surface and tail regions.

In addition to the cross sections, we are also interested in the *factorization ratios* r_{AB} defined by

$$\begin{aligned} r^T_{AB} &= (\sigma^T_{AB})^2/\sigma^T_{AA}\sigma^T_{BB}\,, \\ r^R_{AB} &= (\sigma^R_{AB})^2/\sigma^R_{AA}\sigma^R_{BB}\,, \\ r^E_{AB} &= (\sigma^E_{AB})^2/\sigma^E_{AA}\sigma^E_{BB}\,, \\ r^b_{AB} &= (b_{AB})^2/b_{AA}b_{BB}\,. \end{aligned} \tag{2.8}$$

The factorization hypothesis, as usually formulated in high energy physics, refers to the ratio r^T_{AB} of *total* cross sections; *strict factorization* means $r^T_{AB}=1$. One of the main purposes of the present paper is to investigate to what extent the factorization hypothesis applies to real nucleus-nucleus collisions. In the simple *geometrical* picture which we have outlined above, all of the quantities r_{AB} are on the same footing. Qualitatively, we find that the degree to which factorization is satisfied is much the same for each of the quantities $r^{T,R,E,b}_{AB}$.

III. NUCLEON-NUCLEON AMPLITUDE AND NUCLEAR DENSITIES

The values of σ^T_{NN} and β_{pp} which we use are shown in Table I. The values for $0.52 \leq E_{\rm lab} \leq 7.0$ GeV are obtained from Ref. 13 and the values at 25 GeV from Ref. 14. In each of these cases, we assumed $\beta_{np}=\beta_{pp}$. At 0.1 GeV, σ^T_{NN} and β were calculated directly from NN phase shifts,[15] including s, p, and d waves. In this case, $\beta_{np}=1.18$.

For the nuclear densities ρ_A and ρ_B, we employ parametric representations obtained from analyses of electron scattering data[16] and assume that the mass and charge distributions are proportional. For the light nuclei ^{3}He, ^{12}C, ^{14}N, and ^{16}O, we use a modified Gaussian form[16]

$$\rho(r) = C(1+\alpha k^2\zeta^2)e^{-k^2\zeta^2}\,, \tag{3.1}$$

where $k=[3(2+5\alpha)/2(2+3\alpha)]^{1/2}$, $\zeta = r/R$, R is the rms radius, and C is a normalization constant. For the other nuclei a three parameter Fermi distribution is employed[16]:

$$\rho(r) = C(1+wr^2/R_0^2)/[1+e^{(r-R_0)/a}]\,. \tag{3.2}$$

The parameters α and R of Eq. (3.1) and the parameters w, R_0, and a of Eq. (3.2) are tabulated in Table II. The rms radius R corresponding to the parameter R_0 is also shown in Table II for densities of type (3.2).

TABLE III. Calculated cross sections and elastic slopes at 1.05 GeV/particle.

Reaction $A+B$	x	σ^R_{AB} (b)	$\sigma^T_{AB}/\sigma^R_{AB}$	b_{AB} (fm^2)
$\alpha+^{208}$Pb	0.312	2.58	1.78	19.24
$\alpha+^{90}$Zr	0.399	1.66	1.72	12.43
^{12}C$+^{208}$Pb	0.450	3.39	1.82	25.37
^{14}N$+^{208}$Pb	0.452	3.46	1.82	25.93
$\alpha+^{58}$Ni	0.458	1.28	1.70	9.57
^{16}O$+^{208}$Pb	0.501	3.70	1.82	27.71
^{12}C$+^{90}$Zr	0.576	2.32	1.77	17.31
^{14}N$+^{90}$Zr	0.578	2.38	1.78	17.77
$\alpha+^{16}$O	0.622	0.68	1.58	5.31
^{40}Ar$+^{208}$Pb	0.627	4.81	1.83	36.06
^{16}O$+^{90}$Zr	0.641	2.58	1.78	19.20
^{12}C$+^{58}$Ni	0.662	1.85	1.76	13.76
^{14}N$+^{58}$Ni	0.665	1.90	1.77	14.14
$\alpha+^{12}$C	0.692	0.56	1.55	4.47
^{16}O$+^{58}$Ni	0.737	2.07	1.77	15.44
^{90}Zr$+^{208}$Pb	0.776	5.86	1.85	44.12
^{40}Ar$+^{90}$Zr	0.802	3.49	1.79	26.06
^{120}Sn$+^{208}$Pb	0.845	6.40	1.86	48.28
^{12}C$+^{16}$O	0.898	1.10	1.67	8.27
^{14}N$+^{16}$O	0.902	1.14	1.69	8.56
^{90}Zr$+^{120}$Sn	0.918	4.86	1.84	36.51
^{40}Ar$+^{58}$Ni	0.922	2.89	1.78	21.57
^{3}He$+\alpha$	0.966	0.26	1.35	2.51
^{14}N$+^{12}$C	0.996	0.98	1.67	7.38

IV. CROSS SECTIONS AND ELASTIC SLOPES

In Table III, we show a selection of our numerical results for σ^R_{AB}, σ^T_{AB}, and b_{AB} at 1.05 GeV per particle. The reactions are ordered according to the parameter $x=\min(R_A/R_B, R_B/R_A)$, where R_A

and R_B are the rms radii of the colliding nuclei, listed in Table II.

Several points are to be noted about the results of Table III, which are very similar to our results at other incident energies:

(a) The reaction cross sections σ_{AB}^R are generally quite close to a geometric limit $\pi(R_A^{EQ}+R_B^{EQ})^2$ where $R_A^{EQ}=(\frac{5}{3})^{1/2}R_A$ is the equivalent spherical radius[16] (i.e., the radius of a uniform distribution having the same rms radius) and R_A is the rms radius. This corresponds to our most naive expectation on the basis of two colliding black spheres.

(b) The ratio of total cross section to reaction cross section is generally of order 1.7–1.8, except for collisions between two relatively light nuclei. This is close to the geometric limit of 2.

(c) The elastic slopes b_{AB} are close to the limit $b_{AB}\approx\frac{1}{4}(R_A^{EQ}+R_B^{EQ})^2$, which one would expect on the basis of the black sphere model, for which

$$\frac{d\sigma_{AB}^E/dt}{(d\sigma_{AB}^E/dt)_{t=0}}=4\left|\frac{J_1(qR_{AB})}{qR_{AB}}\right|^2,$$

$$R_{AB}=R_A^{EQ}+R_B^{EQ}, \tag{4.1}$$

$$b_{AB}=\lim_{t\to 0}\frac{1}{t}\ln\left[4\left|\frac{J_1(qR_{AB})}{qR_{AB}}\right|^2\right]$$

$$=(R_A^{EQ}+R_B^{EQ})^2/4.$$

If we assume that $R_A=\tilde{r}_0A^{1/3}$, then in the geometrical limit we expect

$$\sigma_{AB}^T\cong 2\pi r_0^2(A^{1/3}+B^{1/3})^2 \tag{4.2}$$

TABLE IV. Proton-nucleus cross sections and elastic slopes at 800 MeV.

Reaction	σ_{AB}^R (b)	$\sigma_{AB}^T/\sigma_{AB}^R$	b_{AB} (fm^2)
$p+{}^3$He	0.093	1.18	1.38
$p+\alpha$	0.108	1.24	1.37
$p+{}^6$Li	0.174	1.20	2.38
$p+{}^9$Be	0.223	1.28	2.50
$p+{}^{12}$C	0.267	1.33	2.64
$p+{}^{14}$N	0.289	1.38	2.71
$p+{}^{16}$O	0.340	1.36	3.25
$p+{}^{18}$O	0.361	1.38	3.33
$p+{}^{24}$Mg	0.449	1.41	3.98
$p+{}^{28}$Si	0.498	1.43	4.34
$p+{}^{32}$S	0.554	1.44	4.86
$p+{}^{40}$Ar	0.637	1.47	5.42
$p+{}^{48}$Ti	0.715	1.51	5.83
$p+{}^{58}$Ni	0.785	1.55	6.18
$p+{}^{68}$Zn	0.943	1.54	7.565
$p+{}^{90}$Zr	1.068	1.60	8.26
$p+{}^{120}$Sn	1.285	1.63	9.83
$p+{}^{140}$Ce	1.414	1.66	10.69
$p+{}^{197}$Au	1.723	1.70	12.91
$p+{}^{208}$Pb	1.815	1.70	13.62

with $r_0^2=\frac{5}{3}\tilde{r}_0^2$. In Fig. 1, we show the calculated total cross sections at 2.1 GeV. The points correspond to the reactions listed in Table III. The solid curve represents the geometrical approximation of Eq. (4.2), with r_0 adjusted to correctly reproduce the cross sections for the heaviest nuclei. Since $\tilde{r}_0$ is of the order of 1 fm, we expect $r_0\approx(\frac{5}{3})^{1/2}\approx 1.29$ fm, which is close to the value $r_0=1.27$ fm used in Fig. 1.

We have also calculated proton-nucleus cross sections as a function of energy. Note that our proton-nucleus calculations can either be regarded as the folding of the extended proton density of Table II together with a zero range interaction or as the folding of a point proton together with a finite range Gaussian interaction. This latter interpretation is to be preferred, but the numerical calculations are identical. Some typical results are given in Table IV for a proton energy of 800 MeV. This table may be of some qualitative interest to experimentalists engaged in intermediate energy proton-nucleus scattering at the Clinton P. Anderson Meson Physics Facility (LAMPF). We note that one only approaches the geometric limit $\sigma_{AB}^T/\sigma_{AB}^R=2$ for heavy targets. Thus for light targets, we expect the scattering to be more sensitive to the

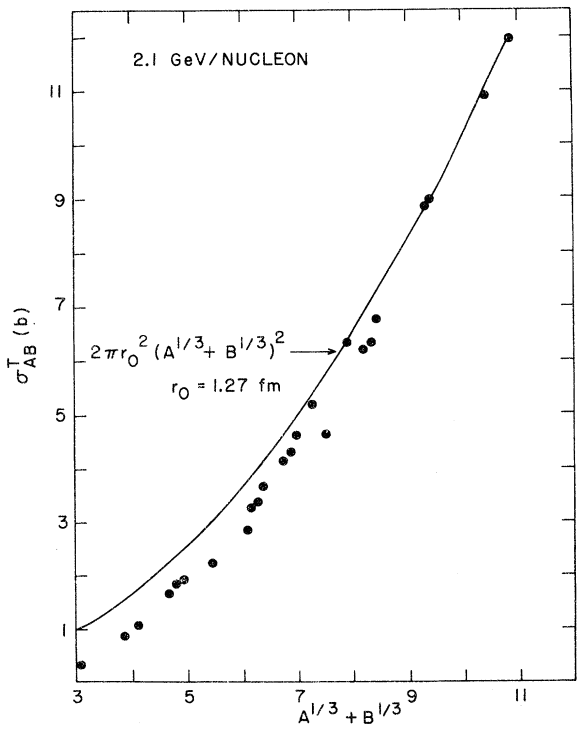

FIG. 1. Total nucleus-nucleus cross sections σ_{AB}^T at 2.1 GeV per particle, as a function of $A^{1/3}+B^{1/3}$. The points correspond to the calculations listed in Table III. The solid curve represents the geometrical approximation of Eq. (4.2).

whole nuclear volume, and hence, $\sigma_{pB}^{T} \propto B$ for relatively small B. For heavier targets, the stronger absorption restricts the proton's interaction to the surface region, and hence, $\sigma_{pB}^{T} \propto B^{2/3}$ for large B. These features are indicated in Figs. 2(a) and 2(b); one sees clearly the change from a volume to a surface reaction as we increase B.

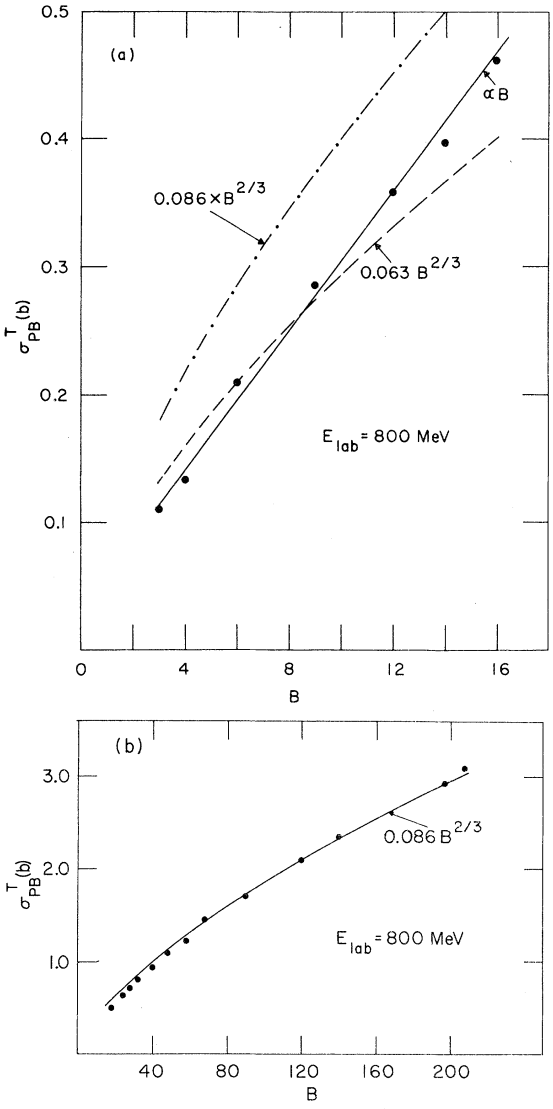

FIG. 2 (a). Calculated proton-nucleus total cross sections σ_{pB}^{T} at 800 MeV lab energy for light targets ($B \lesssim 16$). The heavy dots correspond to the *calculated* reactions listed in Table IV. The solid straight line is a visual fit to indicate dependence on the total number of nucleons of the target. The dashed-dot curve is an extension of the fit to heavy targets while the dashed curve is an attempt to fit the light targets to a $B^{2/3}$ dependence. (b) Calculation of σ_{pB}^{T} at 800 MeV lab energy for medium and heavy targets ($B > 16$). The heavy dots correspond to the *calculated* results listed in Table IV. The solid curve is a visual fit to the heavy target results.

The energy dependence of the cross sections in the region 0.1–25 GeV/particle is shown in Fig. 3 for three typical reactions. They are nearly constant in spite of large variations in β. This lack of sensitivity to β arises because σ_{NN}^{T} is sufficiently large to force all results to lie close to the geometric limit. Equivalently, if the optical potential is very absorptive (close to the black sphere limit), there is little sensitivity to the real part of the potential, within reasonable limits. A quantitative criterion for a "sufficiently large" σ_{NN}^{T} will be discussed in Sec. VI.

V. FACTORIZATION RATIOS

In the geometric limit, the cross sections and elastic slope all vary as $(R_A^{EQ} + R_B^{EQ})^2$ and hence, all the ratios r will be close to the limit

$$r^G = (1+x)^4/16x^2 . \tag{5.1}$$

In Fig. 4, we plot the calculated ratios r as a function of x at 1.05 GeV.[17] The limit r^G is shown for comparison, and is seen to provide a semiquantitative account of the calculated results. Note that for small x, the deviations from strict factorization are quite large. However, if $\frac{2}{3} \leq x \leq 1$ (i.e., the nuclei do not differ in radius by more than 50%), the deviations from strict factorization are seen to be $\leq 20\%$. This is essentially the region of x considered by Fishbane and Trefil.[5]

In Table V, we show the values of r for proton-nucleus interactions at 800 MeV. As x becomes smaller, order of magnitude deviations from strict factorization occur. As in the case of the

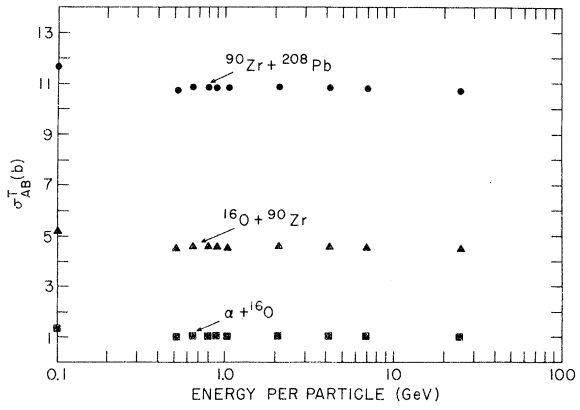

FIG. 3. Predicted energy dependence of nucleus-nucleus total cross sections in the energy range 0.1–25 GeV per particle. The points correspond to the energies and elementary cross sections listed in Table I. Three typical reactions have been chosen from Table III.

TABLE V. Proton-nucleus factorization ratios at 800 MeV.

Reaction	x	r^T	r^R	r^E	r^b	r^G
$p+{}^3$He	0.452	1.14	1.24	0.80	1.67	1.36
$p+\alpha$	0.468	1.24	1.34	1.05	1.55	1.33
$p+{}^6$Li	0.332	1.42	1.67	0.88	2.36	1.78
$p+{}^9$Be	0.331	1.82	2.08	1.55	2.18	1.79
$p+{}^{12}$C	0.324	2.27	2.49	2.38	2.10	1.83
$p+{}^{14}$N	0.323	2.55	2.70	3.02	2.06	1.84
$p+{}^{16}$O	0.291	2.77	3.00	3.10	2.37	2.05
$p+{}^{18}$O	0.289	3.03	3.20	3.70	2.36	2.06
$p+{}^{24}$Mg	0.264	3.74	3.82	5.01	2.63	2.29
$p+{}^{28}$Si	0.256	4.16	4.15	5.93	2.75	2.37
$p+{}^{32}$S	0.256	4.46	4.42	6.46	2.96	2.37
$p+{}^{40}$Ar	0.233	5.25	5.03	8.28	3.17	2.66
$p+{}^{48}$Ti	0.222	6.28	5.78	10.90	3.35	2.83
$p+{}^{58}$Ni	0.215	7.44	6.59	13.98	3.55	2.95
$p+{}^{68}$Zn	0.196	8.17	7.33	15.00	4.09	3.33
$p+{}^{90}$Zr	0.186	10.15	8.58	20.83	4.44	3.57
$p+{}^{120}$Sn	0.172	12.48	10.23	27.10	5.15	3.99
$p+{}^{140}$Ce	0.165	14.50	11.55	33.09	5.65	4.23
$p+{}^{197}$Au	0.150	18.31	13.98	44.59	6.69	4.86
$p+{}^{208}$Pb	0.146	19.14	14.56	46.88	6.98	5.06

nucleus-nucleus results in Fig. 4, the proton-nucleus factorization ratios of Table V exhibit two evident features: (a) the ratios r (except for $p+\alpha$) *exceed* r^G; (b) the values of r are always greater than unity. Observation (b) is a direct consequence of (a), since r^G has the property

$$r^G(x)>1 \quad \text{for } \textit{all } 0<x<1 \tag{5.2}$$

and $r^G=1$ *only* for $x=1$. An experimental ratio $r<1$ would then indicate the failure of the simple geometric picture.

The transition from $r>r^G$ for small x to $r\approx r^G$ for x close to unity can be understood in terms of the following identity:

$$\begin{aligned} r_{AB} &= r^G_{AB}\gamma_{AB}{}^2/\gamma_{AA}\gamma_{BB}\,, \\ \gamma_{AB} &= \sigma_{AB}/\sigma^G_{AB}\,, \end{aligned} \tag{5.3}$$

where r_{AB} refers to r^T_{AB}, r^R_{AB}, or r^E_{AB}, and σ^G_{AB} is the appropriate geometrical limit. In the situation where A is a smaller and lighter nucleus than B, we have $\gamma_{AA}<\gamma_{AB}<\gamma_{BB}$. Introducing the definitions $\gamma_{AA}=\gamma_{AB}(1-\delta_A)$ and $\gamma_{BB}=\gamma_{AB}(1+\delta_B)$, we have

$$r_{AB}/r^G_{AB}=(1-\delta_A)^{-1}(1+\delta_B)^{-1}\,, \tag{5.4}$$

where $\delta_A>0$ and $\delta_B>0$. If we consider the case where the AB and BB cross sections are close to the geometric limit, and AA is relatively far from being geometric, we have $\delta_B<\delta_A$ and hence, $r_{AB}/r^G_{AB}>1$ from Eq. (5.4). This is indeed the

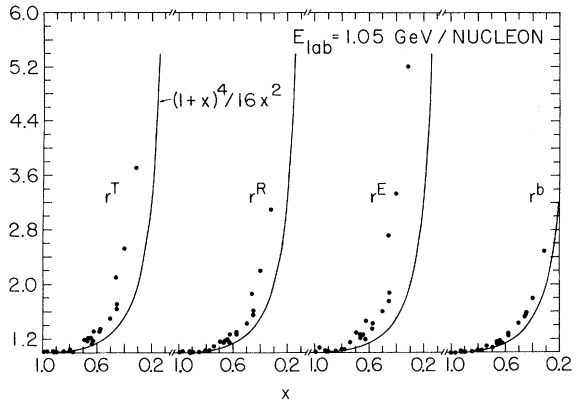

FIG. 4. Factorization ratios r^T, r^R, r^E, and r^b of Eq. (2.8) at 1.05 GeV per particle as a function of the relative size parameter x. The points correspond to the reactions listed in Table III. The solid curves represent the geometrical limit r^G of Eq. (5.1).

situation when A is a very light nucleus (^{3}He or α) and B is a considerably heavier nucleus. The failure of strict factorization is accentuated by the fact that $r_{AB}>r^G_{AB}$, since r^G_{AB} already considerably exceeds unity for small x. As nucleus A becomes larger and comparable in size to nucleus B, we get $\delta_A\approx\delta_B\approx\delta$, and hence, $r_{AB}/r^G_{AB}\approx 1+0(\delta^2)$, i.e., the corrections *linear* in δ cancel if $\delta_A=\delta_B$. Thus, we see that $r_{AB}/r^G_{AB}\to 1$ at the same time that $r^G_{AB}\to 1$. It should be noted that a similar cancellation between terms linear in δ_A and δ_B also occurs in the opposite extreme, where both A and B are very light nuclei. This provides an explanation for the fact that r^T, r^R, and r^E are close to unity for the reaction $^3\text{He}+\alpha$, even though the individual cross sections are relatively far from the geometric limit.

VI. FACTORIZATION RESULTS AS A FUNCTION OF THE ELEMENTARY *NN* CROSS SECTION

The previous discussion has been expressed in terms of a *single* geometrical parameter x. Another parameter which enters the theory is

$$y_{AB}=AB\sigma^T_{NN}/\sigma^G_{AB}\,, \tag{6.1}$$

where $\sigma^G_{AB}\equiv 2\pi(R^{EQ}_A+R^{EQ}_B)^2$. In a real situation, σ^T_{NN} is known and hence y_{AB} is fixed for a given reaction. For the cases in Table III, y_{AB} ranges from 0.3 for $^3\text{He}+{}^3\text{He}$ to 150 for $^{208}\text{Pb}+{}^{208}\text{Pb}$. However, it is of some interest from the point of view of elementary particle physics to study how the composite particle cross sections and factorization ratios depend on y for fixed x.

For $\beta=0$, we have

$$\sigma_{AB}^{T}=4\pi\int_0^\infty (1-e^{-\Delta(b)})\,b\,db\ ,$$

$$\sigma_{AB}^{R}=2\pi\int_0^\infty (1-e^{-2\Delta(b)})\,b\,db\ ,$$

$$b_{AB}=(2\pi/\sigma_{AB}^{T})\int_0^\infty (1-e^{-\Delta(b)})\,b^3\,db\ ,$$

$$\Delta(b)\equiv\sigma_{NN}^{T}\,T(b)/2\ . \tag{6.2}$$

Now let us examine the case of a "weak" elementary cross section σ_{NN}^{T}. We can then expand the exponential factor in Eq. (6.2) for all b. Since in most cases $T(b)$ is a monotonically decreasing function of b, such an expansion is valid if $\Delta(0)\ll 1$. Consider an illustrative example for which the nuclear densities $\rho_{A,B}(r)$ are simulated by Gaussian functions with the correct rms radii $R_{A,B}$

$$\rho_{A,B}(r)=C_{A,B}\,e^{-\gamma_{A,B}r^2}\ ,$$
$$C_{A,B}=(\gamma_{A,B}/\pi)^{3/2}\times\begin{cases}A\\B\end{cases}\ , \tag{6.3}$$
$$\langle r^2\rangle_{A,B}^{1/2}=R_{A,B}=(\tfrac{3}{2}\gamma_{A,B})^{1/2}\ .$$

With the choice (6.3), we have

$$T_{AB}(b)=\frac{AB\xi_{AB}}{\pi}\,e^{-\xi_{AB}b^2}\ ,$$

$$\xi_{AB}=\frac{\gamma_A\gamma_B}{\gamma_A+\gamma_B}=\tfrac{3}{2}\left[\langle r^2\rangle_A+\langle r^2\rangle_B\right]^{-1}\ . \tag{6.4}$$

The requirement $\Delta(0)\ll 1$ is then equivalent to the condition

$$3AB\sigma_{NN}^{T}/\tilde{\sigma}_{AB}^{G}\ll 1\ , \tag{6.5}$$

where $\tilde{\sigma}_{AB}^{G}=2\pi(R_A^2+R_B^2)$. Similar results hold if we assume that $T(b)$ has exponential behavior for large b. For example, if

$$T(b)=\frac{AB}{2\pi}\,\eta^2 e^{-\eta b}\ ,$$
$$\eta=(R_A^{EQ}+R_B^{EQ})^{-1} \tag{6.6}$$

the condition (6.5) is replaced by $y_{AB}/2\ll 1$, where y_{AB} is given by Eq. (6.1). Using Eq. (6.2) and the normalization condition $\int_0^\infty T_{AB}(b)\,b\,db=AB/2\pi$, we obtain

$$\sigma_{AB}^{T}\approx\sigma_{AB}^{R}\approx AB\sigma_{NN}^{T} \tag{6.7}$$

for $y_{AB}\ll 1$. This is just the single scattering approximation to the full multiple scattering series represented by Eq. (6.2). From Eq. (6.7), we see that the condition $y_{AB}\ll 1$ is equivalent to

$$\sigma_{AB}^{T}/\sigma_{AB}^{G}\ll 1\ . \tag{6.8}$$

In the single scattering limit, the total elastic cross section σ_{AB}^{E} vanishes to first order in σ_{NN}^{T}. To second order, we have

$$\sigma_{AB}^{E}\approx\frac{\pi(\sigma_{NN}^{T})^2}{2}\int_0^\infty [T_{AB}(b)]^2 b\,db\ . \tag{6.9}$$

For the exponential and Gaussian approximations of Eqs. (6.4) and (6.6), we find, respectively:

$$\sigma_{AB}^{E}\approx\begin{cases}y_{AB}^2\sigma_{AB}^{G}/16\\3\tilde{y}_{AB}^2\tilde{\sigma}_{AB}^{G}/4\end{cases}\ , \tag{6.10}$$

where $\tilde{y}_{AB}=AB\sigma_{NN}^{T}/\tilde{\sigma}_{AB}^{G}$. From (6.10), we get

$$(r_{AB}^{E})^{-1}=\begin{cases}r_{AB}^{G}\\\tilde{r}_{AB}^{G}\end{cases}\ . \tag{6.11}$$

where $\tilde{r}_{AB}^{G}=(1+x^2)^2/4x^2$ and r_{AB}^{G} is given by Eq. (5.1).

The corresponding elastic slopes

$$b_{AB}=\begin{cases}12b_{AB}^{G}\\\frac{4}{3}\tilde{b}_{AB}^{G}\end{cases} \tag{6.12}$$

for the exponential and Gaussian cases, respectively, where $b_{AB}^{G}=\frac{1}{4}(R_A^{EQ}+R_B^{EQ})^2$ and $\tilde{b}_{AB}^{G}=\frac{1}{4}(R_A^2+R_B^2)$. From Eq. (6.12) we get

$$r_{AB}^{b}=\begin{cases}r_{AB}^{G}\\\tilde{r}_{AB}^{G}\end{cases}\ . \tag{6.13}$$

It is amusing that the limit r_{AB}^{G} also applies to r_{AB}^{E} and r_{AB}^{b} in the limit $y_{AB}\ll 1$, even though the total cross section is much smaller than its geometric limit, as per Eq. (6.8). From Eqs. (6.11) and (6.13), we have the following property in the "weak" σ_{NN}^{T} limit:

$$r_{AB}^{b}\,r_{AB}^{E}\to 1\ \text{ as } y_{AB}\to 0. \tag{6.14}$$

Now let us consider the opposite extreme, where the elementary cross section is strong, i.e., $\Delta(0)\gg 1$. However, we must have $\Delta(b)\ll 1$ for sufficiently large b. The impact parameter integral can then be divided up into three regions:

$$\int_0^\infty (1-e^{-\Delta(b)})\,b\,db\approx\int_0^{b_0} b\,db+\int_{b_0}^{b_1}(1-e^{-\Delta(b)})\,b\,db$$
$$+\int_{b_1}^\infty \Delta(b)\,b\,db\ , \tag{6.15}$$

where b_0 and b_1 are determined by the conditions

$$\Delta(b_0)=\bar{\alpha}\gg 1\ ,$$
$$\Delta(b_1)=\bar{\beta}\ll 1\ . \tag{6.16}$$

We now use the fact that $1-e^{-x}<x$ for all $x>0$

to obtain an upper bound

$$\int_{b_0}^{b_1} (1 - e^{-\Delta(b)}) b\, db < \int_{b_0}^{b_1} \Delta(b) b\, db \ .$$

We then have

$$\int_0^{\infty} (1 - e^{-\Delta(b)}) b\, db \lessapprox \int_0^{b_0} b\, db + \int_{b_0}^{\infty} \Delta(b) b\, db \ . \tag{6.17}$$

For large σ_{NN}^T, the second term is small compared to the first, and we get the rough estimate

$$\sigma_{AB}^T \approx 2\sigma_{AB}^R \approx 2\sigma_{AB}^E \approx 2\pi b_0^2 \ . \tag{6.18}$$

Using Eq. (6.16) to determine b_0, we find for

$$\sigma_{AB}^T \approx \begin{cases} \sigma_{AB}^G [\ln(y_{AB}/\tilde{\alpha})]^2 \\ \frac{2}{3} \tilde{\sigma}_{AB}^G \ln(3\tilde{y}_{AB}/\tilde{\alpha}) \end{cases} \tag{6.19}$$

for exponential or Gaussian densities, respectively. Note that (6.19) implies that although $\sigma_{AB}^T \to \infty$ as $\sigma_{NN}^T \to \infty$, the ratio $\sigma_{AB}^T / \sigma_{NN}^T \to 0$. The fact that σ_{AB}^T can exceed σ_{AB}^G by an arbitrary amount is due to the fact that we have assumed nuclear densities with exponential or Gaussian tails which extend to infinity. If we use a *sharp cutoff* model with $\rho_{A,B}(r) = 0$ for $r > R_{A,B}^{EQ}$, then σ_{AB}^T does not exceed σ_{AB}^G. The same reasoning applies to the elastic slopes b_{AB}. We find

$$b_{AB} \approx \begin{cases} b_{AB}^G [\ln(y_{AB}/\tilde{\alpha})]^2 \\ \frac{2}{3} \tilde{b}_{AB}^G \ln(3\tilde{y}_{AB}/\tilde{\alpha}) \end{cases} \ . \tag{6.20}$$

Thus, for strong σ_{NN}^T, all factorization ratios are given by:

$$r_{AB}^T \approx r_{AB}^R \approx r_{AB}^E \approx r_{AB}^b \approx \begin{cases} r_{AB}^G \\ \tilde{r}_{AB}^G \end{cases} \ . \tag{6.21}$$

Note that the exact value of the geometric limit depends on the form of the nuclear densities for large r. The difference between an exponential (realistic) and a Gaussian tail for $\rho_{A,B}(r)$ shows up as a considerable difference in the geometric limit, i.e., $\tilde{r}_{AB}^G \approx 4 r_{AB}^G$ for $x \ll 1$.

In Fig. 5, we show the calculated dependence of the factorization ratios r on the parameter y_{AB} of Eq. (6.1). For definiteness, we have chosen the $\alpha + {}^{208}$Pb reaction at 2.1 GeV/particle, with densities of Table II. Several features are to be noted:
(a) For large σ_{NN}^T, all factorization ratios approach a value very close to the naive geometrical limit r_{AB}^G, for exponential $T(b)$, as per Eq. (6.21).
(b) For small σ_{NN}^T, the calculated total cross sections approach $AB\sigma_{NN}^T$, and we further have $r_{AB}^T \approx r_{AB}^R \approx 1$ and $r_{AB}^E r_{AB}^b \approx 1$, as per Eq. (6.14).
(c) For y_{AB} of the order of 1, very large deviations from strict factorization occur, particularly for r^E. In the context of Eq. (5.4), these situations correspond to $\delta_A \gg \delta_B$, i.e., the AA cross section is very far from the geometric limit and hence, $r \propto \sigma_{AA}^{-1}$ is large.
(d) The actual value of y_{AB} is 6.73 for the $\alpha + {}^{208}$Pb reaction at 2.1 GeV/particle. Thus we are closer to the "strong" than to the "weak" limit. However, for this case, we are still relatively far from the strict geometric limit, although a description in terms of r_{AB}^G is qualitatively correct. From Fig. 5, we see why the calculated values of r^T, r^R, r^E, and r^b lie *above* the limit r^G for the wide range of reactions shown in Fig. 4; i.e., the ratios r always approach r^G from above as we increase y.

VII. CONCLUSIONS

In this paper we have presented numerical results for nucleus-nucleus cross sections at intermediate and high energies. These results, which are based upon the eikonal representation

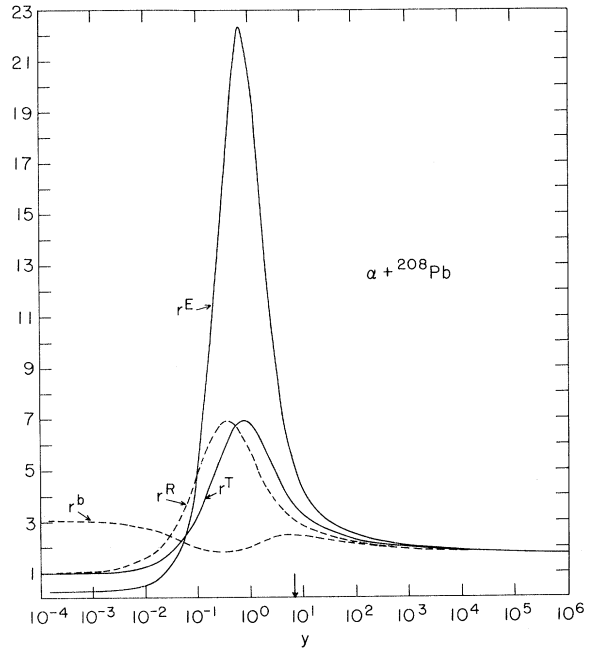

FIG. 5. Dependence of the factorization ratios r^T, r^R, r^E, and r^b on the geometricity parameter y of Eq. (6.1) for the $\alpha + {}^{208}$Pb reaction at 2.1 GeV per particle. The case $y \ll 1$ corresponds to the single scattering limit of Eq. (6.7) while $y \gg 1$ yields the geometric limit of Eq. (6.21). The actual value of y for this case is indicated by an arrow.

of the scattering amplitude for composite particles and on the relatively short range of the basic nucleon-nucleon interaction, are directly testable in the initial stages of the experimental programs at the new generation of facilities such as the Bevalac, LAMPF, TRIUMF, and SIN. Such studies can delineate the gross features of nucleus-nucleus interactions at high energies, and could confirm that the above elements provide a framework for their understanding.

Within the above framework, we have investigated the degree to which cross section and elastic slope ratios as in Eq. (2.8) exhibit a *numerical* factorization property, i.e., are close to unity. We have shown that this holds to 20% if the radii of the projectile and target nuclei do not differ by more than 50%. This leads us to the conjecture, with particular reference to nucleus-nucleus collisions, that an approximate factorization of cross sections and elastic scattering slopes is a geometric property of the scattering of spatially extended strongly interacting particles of *similar size*.

We believe that nucleus-nucleus factorization ratios will be interpretable in terms of the simple geometric limit given by Eq. (5.1). Deviations from Eq. (5.1) can also be understood via Eqs. (5.3) and (5.4) in terms of the deviations of cross sections from the geometric limit. Geometrical behavior follows because the basic nucleon-nucleon interaction is of relatively short range and is strong, leading to a large absorptive part for the nucleus-nucleus potential. Because of the strong absorption, nucleus-nucleus elastic scattering is a peripheral process and the situation is relatively close to the limit of black sphere scattering. The simple representation (2.1) for the nucleus-nucleus amplitude should be applicable at the energies per particle attainable with present facilities. However, it is possible that the representation (2.1)–(2.3) does not apply at ultrahigh energies, for which scales of distance other than the relative size of the nuclei may enter in an essential way. For example, if the range of the basic nucleon-nucleon interaction increases with energy and ultimately becomes very large compared to the radii of the nuclei, while at the same time σ_{NN}^{T} does not increase in a similar way, one can regain[5,6] the single scattering result $\sigma_{AB}^{T} = AB\sigma_{NN}^{T}$. Thus strict functional factorization could emerge at *extremely* high energies.[6] However, this is very speculative since in the highest energy experiments presently avaiable,[18] the slowly shrinking pp diffraction pattern goes as $d\sigma^{E}/dt \sim \exp(-13|t|)$, corresponding to a size $R \approx \frac{1}{2} m_{\pi} \approx 0.7$ fm. This size is still significantly smaller than the radii of even the lightest nuclei. Furthermore, in this energy domain the basic cross section has begun to increase.[18]

---

*Work supported in part by the U.S. Atomic Energy Commission.

†Research supported, in part, by the U.S. Atomic Energy Commission under Contract No. AT(11-1)-3001.

[1]H. H. Heckman, in *High Energy Physics and Nuclear Structure, Proceedings of the Fifth International Conference on High-Energy Physics and Nuclear Structure, Uppsala, Sweden, 18–22 June 1973,* edited by G. Tibell (North-Holland, Amsterdam/American Elsevier, New York, 1974); also available as Lawrence Berkeley Laboratory Report No. LBL-2052, June, 1973 (unpublished).

[2]H. Steiner, in Lectures at the Adriatic Meeting on Particle Physics, Rovinj, Yugoslavia, September 23–October 5, 1973 (unpublished), Lawrence Berkeley Report No. LBL-2144; G. F. Chew, Comments on Nuclear and Particle Physics 2, 107 (1968); plus various internal Berkeley reports.

[3]W. Czyz and L. C. Maximon, Ann. Phys. (N.Y.) 52, 59 (1969); G. Fäldt, H. Pilkuhn, and H. G. Schaile, *ibid.* 82, 326 (1974); this latter article contains a number of references to earlier work on relativistic nucleus-nucleus collisions; see also A. Tekou, Nucl. Phys. B46, 141, 152 (1972).

[4]T. W. Donnelly, J. Dubach, and J. D. Walecka, Nucl. Phys. A232, 355 (1974).

[5]P. M. Fishbane and J. S. Trefil, Phys. Rev. Lett. 32, 396 (1974).

[6]V. Franco, Phys. Rev. Lett. 32, 911 (1974).

[7]J. Pumplin and G. L. Kane, Phys. Rev. Lett. 32, 963 (1974).

[8]S. Barshay, C. B. Dover, and J. P. Vary, Phys. Lett. 51B, 5 (1974).

[9]R. J. Glauber, in *High Energy Physics and Nuclear Structure,* edited by G. Alexander (North-Holland, Amsterdam, 1967), p. 311.

[10]T. T. Chou and C. N. Yang, Phys. Rev. Lett. 20, 1213 (1968); Phys. Rev. 170, 1591 (1968); 175, 1832 (1968).

[11]A. Dar and Z. Kirzon, Phys. Lett. 37B, 166 (1971); W. L. Wang and R. G. Lipes, Phys. Rev. C 9, 814 (1974).

[12]J. P. Vary and C. B. Dover, Phys. Rev. Lett. 31, 1510 (1973).

[13]D. V. Bugg, D. C. Slater, G. H. Stafford, R. F. George, K. F. Riley, and R. J. Tapper, Phys. Rev. 146, 980 (1966).

[14]K. J. Foley *et al.*, Phys. Rev. Lett. 19, 857 (1967).

[15]M. H. MacGregor, R. A. Arndt, and R. M. Wright, Phys. Rev. 182, 1714 (1969), Table VI.

[16]H. R. Collard, L. R. B. Elton, and R. Hofstadter, in *Landolt-Börnstein: Numerical Data and Functional Relationships in Science and Technology,* edited by K.-H. Hellwege and H. Schopper (Springer, Berlin, 1967), Group I, Vol. 2, p. 21 and references therein.

Most density parameters in Table II have been taken directly from these tables. However, for ^{40}Ar, we used the parameters of J. L. Groh, R. P. Singhal, and H. S. Caplan, Can. J. Phys. 49, 2073 (1971); for ^{58}Ni, see J. R. Ficenec, W. P. Trower, J. Heisenberg, and I. Sick, Phys. Lett. 32B, 460 (1970); for ^{90}Zr, see Phan Xuan Ho, J. B. Bellicard, A. Bussiere, P. Leconte, and M. Priou, Nucl. Phys. A179, 529 (1972).

[17]Very similar results at 2.1 GeV/particle are given in Ref. 8.

[18]U. Amaldi, in Highlights in Particle Physics, edited by A. Zichichi (Editrice Compositori, Bologna, Italy, to be published), CERN HP Report No. 73-5.